frontiers in Physics

ORIGINAL RESEARCH
published: 30 March 2022
doi: 10.3389/fphy.2022.843932

Identification of Diffracted Vortex Beams at Different Propagation Distances Using Deep Learning

Heng Lv[1†], *Yan Guo*[1†], *Zi-Xiang Yang*[1], *Chunling Ding*[1], *Wu-Hao Cai*[1], *Chenglong You*[2*] and *Rui-Bo Jin*[1,3*]

[1]Hubei Key Laboratory of Optical Information and Pattern Recognition, Wuhan Institute of Technology, Wuhan, China, [2]Quantum Photonics Laboratory, Department of Physics and Astronomy, Louisiana State University, Baton Rouge, LA, United States, [3]Guangdong Provincial Key Laboratory of Quantum Science and Engineering, Southern University of Science and Technology, Shenzhen, China

The Orbital angular momentum (OAM) of light is regarded as a valuable resource in quantum technology, especially in quantum communication and quantum sensing and ranging. However, the OAM state of light is susceptible to undesirable experimental conditions such as propagation distance and phase distortions, which hinders the potential for the realistic implementation of relevant technologies. In this article, we exploit an enhanced deep learning neural network to identify different OAM modes of light at multiple propagation distances with phase distortions. Specifically, our trained deep learning neural network can efficiently identify the vortex beam's topological charge and propagation distance with 97% accuracy. Our technique has important implications for OAM based communication and sensing protocols.

Keywords: deep learning, vortex beams, orbital angular momentum, propagation, diffraction

OPEN ACCESS

Edited by:
Omar Magana-Loaiza,
Louisiana State University,
United States

Reviewed by:
Tao Peng,
Texas A&M University, United States
Xiangping Li,
Jinan University, China

***Correspondence:**
Chenglong You
cyou2@lsu.edu
Rui-Bo Jin
jrbqyj@gmail.com

[†]*These authors have contributed equally to this work*

Specialty section:
This article was submitted to Quantum Engineering and Technology, a section of the journal Frontiers in Physics

Received: *27 December 2021*
Accepted: *15 February 2022*
Published: *30 March 2022*

Citation:
Lv H, Guo Y, Yang Z-X, Ding C, Cai W-H, You C and Jin R-B (2022) Identification of Diffracted Vortex Beams at Different Propagation Distances Using Deep Learning. Front. Phys. 10:843932. doi: 10.3389/fphy.2022.843932

INTRODUCTION

Vortex beam generally refers to the phase vortex beam, which has a spiral wavefront, a phase singularity in the center of the beam, and ring-shaped intensity distribution [1, 2]. The beam with orbital angular momentum (OAM) has the phase term $e^{i\ell\phi}$ in the complex amplitude equation, where ϕ is the azimuthal angle and ℓ is the angular quantum number or topological charge. OAM is an inherent characteristic of vortex beam photons, and each photon carries OAM, which is $\ell\hbar$ [3, 4]. Due to the high-dimensional characteristics of the photon OAM, it is utilized in applications such as optical tweezers [5, 6], micromanipulation [7, 8], angular velocity sensing [9], quantum information [10–13], quantum computing [14–17], optical communications [18–22] and quantum cryptography [23]. Once the value of ℓ is identified, the orbital angular momentum can be calculated, allowing the features of the vortex beam to be determined. Unfortunately, the vortex beam will diffract during propagation, and its spatial profile will be easily distorted in a real-world environment [24]. Detrimentally, the information encoded in the structured beam can be destroyed by random phase distortions [25–27] and diffraction effects, resulting in mode loss and mode cross-talk [28, 29]. As a result, capturing the vortex beam and identifying its information using equipment such as a charge coupled device (CCD) camera or a complementary metal oxide semiconductor (CMOS) camera is difficult [30]. Hitherto, the traditional methods of identifying vortex beams have included methods such as the interferometer method, plane wave interferometry, and triangular aperture diffraction measurement, to name a few [31–34]. These traditional methods are much more challenging

due to the need for more equipment, as well as complicated data analysis process. In addition, some of these methods can only identify specific vortex beams [35]. Moreover, the accuracy of these methods will be greatly reduced when turbulence is considered. These aforementioned factors have significantly hampered the performance of communication, cryptography, and remote sensing. As a result, identifying OAM efficiently and correctly while accounting for diffraction and turbulence is a critical and unresolved challenge.

In recent years, methods such as deep learning algorithms [36] and transfer learning [37] have considerably increased the accuracy of automatic image recognition [38, 39]. A significant number of recent articles have proved the potential of artificial neural networks for efficient pattern recognition and spatial mode identification [40–42], and its accuracy is far superior to some traditional identification detection methods [43–45]. However, due to the complex diffraction effect in the OAM propagation process, there is little relevant work in the identification of the propagation distance value. In the related research, the propagation distance of the vortex beam ranges from the order of centimeters to the order of kilometers, and it is used as a known parameter [46, 47]. Different propagation distance z will drastically change the size of the central aperture of the vortex beam. As a result, it remains difficult to identify the z value using only the intensity pattern. Additionally, changing the value of topological charge ℓ also changes the size of the central aperture, making the identification task more challenging. Finally, turbulence in real-world applications exacerbates the difficulty of such an identification task [48].

In this report, we take advantage of the deep learning algorithm to identify vortex beams and their propagation distances while considering the effects of undesired turbulence. Through theoretical simulations and experiments, we generated vortex beams with different propagation distances and topological charges. In addition, using the transfer learning method, we designed a deep learning model to classify vortex beams. For the first time, our approach utilizes artificial intelligence to simultaneously identify the propagation distance and topological charge of a vortex beam under turbulence's effects. Our research enables the encoding of vortex beams with different propagation distances. As a result, the vortex beam propagation distance may become a new encoding variable. With the improvement of the accuracy of distance recognition, it is even possible to realize precise distance measurement based on the intensity of vortex beams. Our research opens up a new direction for OAM communication and has great significance in OAM based sensing.

THEORY AND METHODS

Generation of the Vortex Beam

The fundamental beam used to produce the vortex beam is a Gaussian beam. By applying a phase mask on the spatial light modulator (SLM), the beam amplitude on the plane of SLM becomes [49]:

$$E_1(r,\theta) = \exp\left(-\frac{r^2}{\omega_0^2}\right)\exp(-i\ell\theta), \tag{1}$$

where ℓ is the topological charge, ω_0 is the Gaussian beam waist, r and θ are radial and azimuthal coordinates, respectively.

Within the framework of paraxial approximation, the field distribution of $E_1(r,\theta)$ after propagation can be calculated using the Collins integral equation [50]:

$$E_2(r_1,\theta_1,z) = \frac{i}{\lambda B}\exp(-ikz)\int_0^{2\pi}\int_0^{\infty} E_1(r,\theta) \times \exp\left[-\frac{ik}{2B}\left(Ar^2 - 2rr_1\cos(\theta_1-\theta) + Dr_1^2\right)\right] r dr d\theta, \tag{2}$$

where r_1 and θ_1 are radial and azimuthal coordinates in the output plane, z is the propagation distance, and $k = 2\pi/\lambda$ is the wave number with λ being the wavelength. The ABCD transfer matrix of light propagation in free space of distant z is

$$\begin{pmatrix} A & B \\ C & D \end{pmatrix} = \begin{pmatrix} 1 & z \\ 0 & 1 \end{pmatrix}. \tag{3}$$

By inserting **Eq. 1** and **Eq. 3** into **Eq. 2**, we can obtain the beam amplitude as

$$E_2(r_1,\theta_1,z) = \frac{i^{\ell+1}\pi}{\lambda z}\exp(-ikz)\exp\left(-\frac{ikr_1^2}{2z}\right)\exp(-i\ell\theta_1) \frac{b_1^{\ell}}{\varepsilon_1^{1+\frac{\ell}{2}}}\frac{\Gamma\left(\frac{\ell}{2}+1\right)}{\Gamma(\ell+1)}{}_1F_1\left(\frac{\ell+2}{2},\ell+1,-\frac{b_1^2}{\varepsilon_1}\right). \tag{4}$$

Eq. 4 represents the hypergeometric Gaussian mode. ${}_1F_1(\alpha,\beta,z)$ is a confluent hypergeometric function, $\Gamma(n)$ is the Gamma function, b_1 and ε_1 are defined as:

$$b_1 = \frac{kr_1}{2z}, \quad \varepsilon_1 = \frac{1}{\omega_0^2} + \frac{ik}{2z}. \tag{5}$$

Based on the above calculations, we can obtain transverse intensity images of vortex beam with different values of ℓ after propagating different distances z.

In actual communication, turbulence can lead to phase distortion of optical mode spatial distribution. Therefore, in our experiment, we use the Kolmogorov model with Von Karman spectrum of turbulence to simulate the atmospheric turbulence in SLM to achieve a distorted communication mode [51, 52]. The degree of distortion is quantified by the Fried's parameter r_0. The expression of the turbulence phase mask we added on the SLM is [42]:

$$\Phi(x,y) = \mathbb{R}\left\{\mathcal{F}^{-1}\left(\mathbb{M}_{NN}\sqrt{\phi_{NN}(\kappa)}\right)\right\}, \tag{6}$$

with $\phi_{NN}(\kappa) = 0.023 r_0^{-5/3}(\kappa^2+\kappa_0^2)^{-11/6} e^{-\kappa^2/\kappa_m^2}$ and the Fried's parameter $r_0 = (0.423k^2C_n^2 z)^{-3/5}$. The symbol $\mathbb{R}$ represents the real part of the complex field, and $\mathcal{F}^{-1}$ indicates the inverse Fourier transform operation. In addition, κ, κ_0, and $\mathbb{M}_{NN}$ represent the spatial frequency, the central spatial frequency, and encoded random matrix, respectively. C_n^2 is the standard

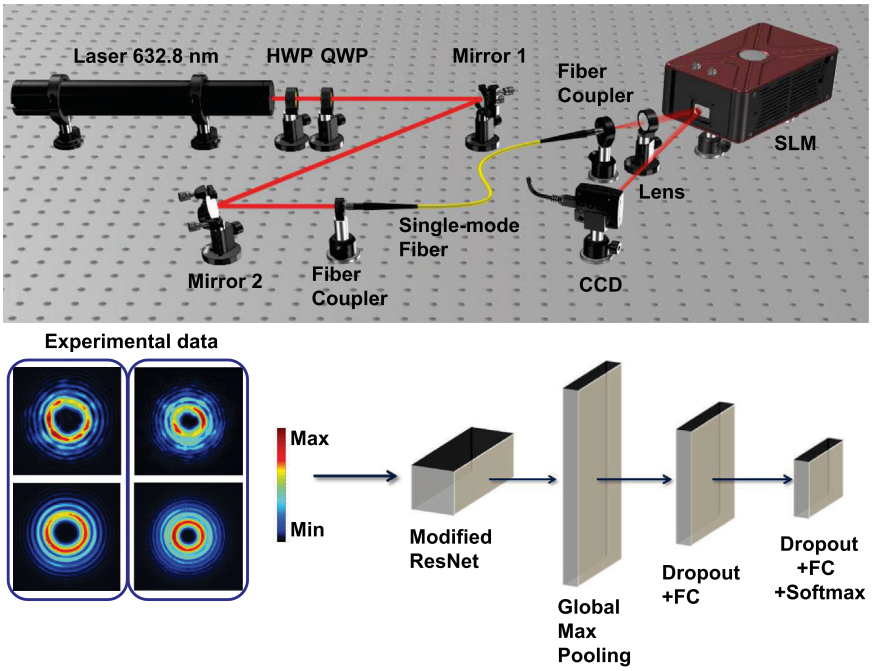

FIGURE 1 | The experimental setup (upper panel) and our customized deep learning algorithm (lower panel). We perform the experiment using a collimated He-Ne laser beam. The vortex beam is generated using an SLM with the computer-generated hologram. Finally, the intensity images are collected by a CCD and used for training and testing. Our deep learning network consists of the unaltered ResNet-101 bottom layer and our redesigned top layer.

refractive index, which is a constant representing the turbulence intensity.

After the turbulence term is added to the original phase mask and loaded on the SLM, beam amplitude on the plane of SLM becomes

$$E_1'(r,\theta) = E_1(r,\theta)\exp\left[i\Phi(x,y)\right]. \tag{7}$$

By substituting **Eq. 7** into **Eq. 2**, we can numerically obtain the field distribution of the turbulence distorted $E_2'(r_1,\theta_1,z)$ after propagation.

The experimental setup and the deep learning model are shown in **Figure 1**. In our experiment, the vortex beams are generated by using an SLM and computer-generated holograms. Utilizing the first-diffraction order of SLM, we can obtain the vortex beam of arbitrary topological charge. A laser beam from a He-Ne laser (wavelength of 632.8 nm) is coupled into a single-mode fiber for spatial mode cleaning. A half-wave plate (HWP) and a quarter-wave plate (QWP) are employed to adjust the polarization of the laser beam at the output port of the fiber. An objective lens (magnification of 10× and an effective focal length of 17 mm) is used to collimate the light from the fiber, and the beam waist after collimation is around 2 mm. By loading a computer-generated phase hologram onto the SLM, a Gaussian beam is converted into a vortex beam. In order to simulate the turbulence in an atmosphere transmission process, we can add an additional turbulence phase to the hologram. Finally, a CCD camera is used to collect the intensity images of the vortex beam, and the transmission distance is controlled by changing the distance between the CCD and the SLM. The images collected by the CCD are sent to a computer for training. Each training set, validation set, and test set contain 86, 10, and 10 images (360 × 360 pixels), in which the value of ℓ ranges from 1 to 5, and the propagation distance z ranges from 40 to 100 cm with a step of 5 cm. Totally, there are 86 × 5 × 13 = 5590 images for the training set and 10 × 5 × 13 = 650 images for the validation set and test set.

The Deep Learning Algorithm

The lower panel of **Figure 1** shows our customized deep learning algorithm model. Our model is a transfer learning network based on the ResNet-101 network design [53]. Since our obtained images have a high degree of similarity, the neural network must have enough depth to extract image features. Therefore, we adopt the CNN architecture and retrain the ResNet-101 deep learning model rather than the shallow neural networks model. More specifically, the top layer is removed from the original ResNet-101. Moreover, a global max pooling layer with a node count of 2048 is used to reduce the parameters to increase the calculation speed. Following that, a dropout layer is added to remove some parameters randomly to minimize over-fitting, and then we use a fully connected (FC) layer to connect the local features. Another dropout layer and an FC layer are added to lower the number of nodes from 1024 to 65. Finally, a softmax layer is applied for a 65 classification probability output.

To train and test the deep learning model, we utilize a computer with an Intel(R) Core(TM) i5-7300HQ CPU @2.5 GHz and an Nvidia GeForce GTX 1050 Ti GPU with

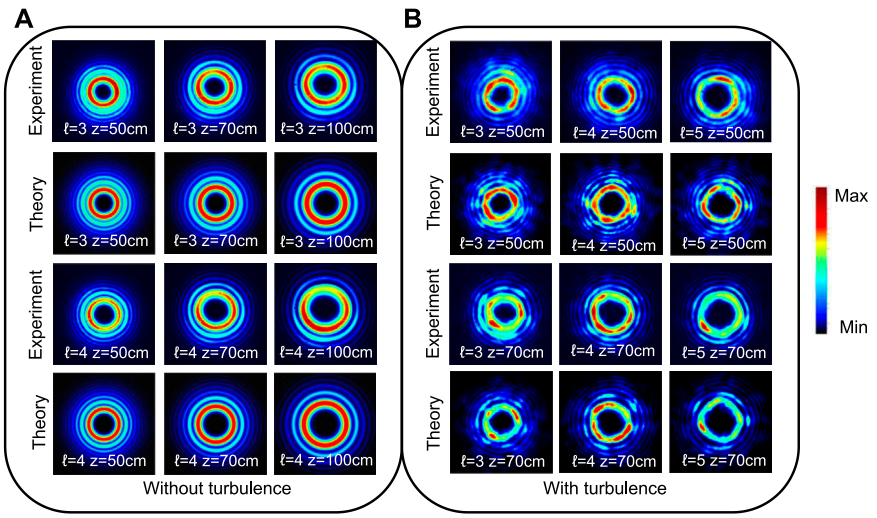

FIGURE 2 | The spatial profiles of different vortex beams. We show the experimentally measured images and simulated images for different topological charges ℓ and different propagation distances z, without turbulence in **(A)** and with turbulence in **(B)**. The first and third rows are the images acquired from the experiment, and the second and fourth rows represent the theoretically simulated images.

4 GB of video memory. We use an adaptive moment estimation (Adam) optimizer throughout the algorithm [54]. In our deep learning model, we also used the transfer learning technique (TLT) [55], which has two benefits. Firstly, it is highly efficient; for example, tasks that originally required months of training without TLT can be reduced to a few hours. The second merit of TLT is that less data is needed. This is because transfer learning requires the use of a pre-trained model, which allows us to achieve accurate recognition results with fewer datasets [56]. Generally speaking, only hundreds or thousands of training images (instead of tens of thousands or even millions of images) are enough to achieve good training results [57, 58]. Finally, the training results in each epoch are evaluated by the categorical cross-entropy loss function [59] which is given by

$$\text{Loss} = -\sum_{i=1}^{n} (\hat{y}_{i1} \ln y_{i1} + \hat{y}_{i2} \ln y_{i2} + \cdots + \hat{y}_{im} \ln y_{im}), \quad (8)$$

where n is the number of samples, m is the number of classifications, $\hat{y}_{im}$ indicates that the true label (with the value of 0 or 1), and y_{im} is the predicted value of the mth class given by the neural network.

RESULTS AND DISCUSSION

Figure 2 shows the spatial profiles of vortex beams with different propagation distances z and topological charges ℓ obtained from experiments and simulations. **Figure 2A** shows the vortex beams without turbulence, and **Figure 2B** depicts vortex beams affected by turbulence. The first and third rows depict the spatial profiles of the vortex beams acquired in the experiment, while the second and fourth rows depict the simulated ones under identical conditions. For simplicity, we define the first aperture in the center as the "center aperture" and other outer apertures as the "diffraction apertures". For a fixed value of ℓ, the size of the central aperture becomes larger as the propagation distance z value increases. At the same time, for a fixed propagation distance z, the size of the central aperture also increases as the value of ℓ increases. From **Figure 2**, we can observe that the spatial profiles obtained from the experiment match well with our simulations, therefore validating our theoretical model of the experiment. By comparing the experimental and theoretical images of $\ell = 4$ and $z = 100$ cm, we can notice that the central aperture in the experimental image is not distributed uniformly. This effect is due to the slight misalignment of the collimated beam to the center of the SLM. As a result, the brightness and shape of the center aperture can vary slightly. This kind of deviation is also included, in order to increase the diversities of the training data. We will show later that, even with such deviations, the training results remain excellent.

There are many situations where the size of the central aperture is comparable for vortex beams with different ℓ and propagation distance z. This particular effect makes the simultaneous identification of ℓ and z difficult. For example, by comparing the theoretical image of $\ell = 3$ and $z = 70$ cm (second row, second column), and the image of $\ell = 4$ and $z = 50$ cm (fourth row, first column) in **Figure 2A**, we can notice that the sizes of the center aperture are similar, making it difficult to distinguish between these two modes. In this case, the difference of the diffraction apertures provides the best characteristic value to distinguish them. More intuitively, **Figure 3** shows the cross-sectional view of the intensity for these two beams at $y = 0$. It is clear that the distance between the two main peaks in **Figure 3A** and **Figure 3B** is almost the same. However, **Figure 3A** has 4 side lobes in the diffraction apertures, while **Figure 3B** has 6 side lobes in the diffraction apertures. This subtle difference makes it possible to distinguish these two cases. Finally, we note that in

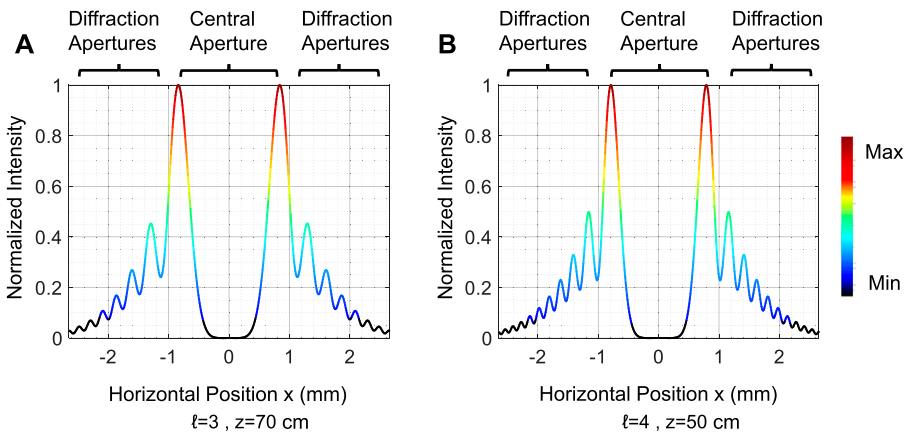

FIGURE 3 | The cross-sectional view of the intensity images at $y = 0$ for **(A)** $\ell = 3, z = 70$ cm and **(B)** $\ell = 4, z = 50$ cm. The size of the central apertures is comparable in both images. However, the number of side lobes in the diffractive apertures is different. This subtle feature enables us to distinguish these two cases.

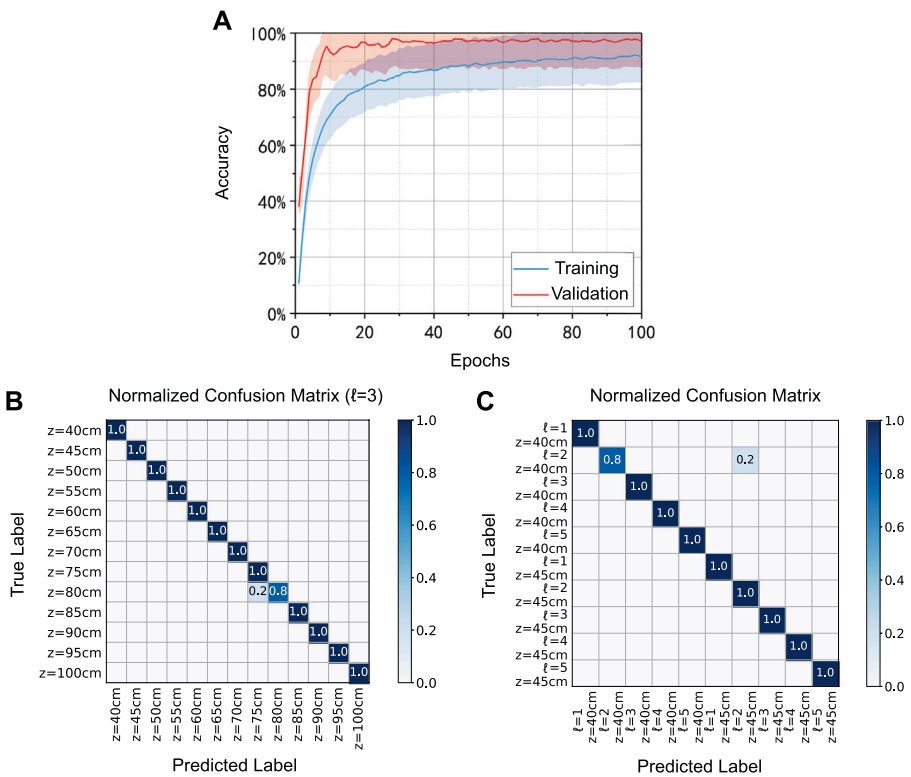

FIGURE 4 | The accuracy and confusion matrix of our trained deep learning algorithm. **(A)** The accuracy of the training set and the validation set versus the epochs. The accuracy of up to 97% is achieved in identifying vortex beams with different ℓ values and different z values after 90 epochs. All shaded areas correspond to the standard deviation of accuracy. All classification results have been tested and verified, and some test results are shown here. **(B)** The normalized confusion matrix between the predicted propagation distance and the true propagation distance for $\ell = 3$. **(C)** Normalized confusion matrix between predicted ℓ values, predicted propagation distance and true ℓ values, true propagation distance.

Figure 3 the diffraction apertures in the region of $|x| > 2.2$ mm (in black) usually cannot be well captured by a CCD in the experiment, due to low light intensity and limited resolution of the CCD.

In practical communication applications, the spatial profile of the vortex beam might be distorted due to atmospheric turbulence, underwater turbulence, or other adverse circumstances. Therefore, the turbulence should be taken into

account for the propagation of the vortex beam. **Figure 2B** shows the typical simulated and experimental diagrams with turbulence. In these theoretical (the second and fourth rows) and experimental (the first and third rows) data, a turbulence intensity parameter of $C_n^2 = 5 \times 10^{-10}$ mm$^{-2/3}$ is utilized. In these data sets, we also take into account the fact that light might not be precisely incident on the center of the SLM plane. It can be noticed that the turbulence created huge distortions on the vortex beam's center aperture and diffraction apertures. For deep learning training, we gathered 1040 distorted light intensity images.

To show the performance of our deep learning network, we plot the accuracy as a function of the training epochs in **Figure 4A**. We can see that after 90 training epochs, the accuracy is higher than 92% for the training set, while the accuracy of the validation set is greater than 97%. Since we added regularization and dropout operations during the training process. These operations will be automatically closed during the verification process, causing the accuracy of the validation set to be higher than the accuracy of the training set. A high validation accuracy of 97% indicates that our approach provides a powerful way to identify the vortex beams with different ℓ values and different z values, even under a turbulent environment. Finally, we note that the number of epochs required for convergence depends on multiple factors, including the number of cases of different vortex beams propagated and the degree of turbulence.

To show our results more comprehensibly, we calculated the normalized confusion matrix for different ℓ and z. **Figure 4B** shows a typical normalized confusion matrix from $\ell = 3$, $z = 40$ cm to $\ell = 3$, $z = 100$ cm. **Figure 4C** shows the normalized confusion matrix from $\ell = 1$, $z = 40$ cm to $\ell = 5$, $z = 45$ cm. The true propagation distance and the predicted propagation distance given by our deep learning algorithm are basically on a diagonal line. The result means almost all OAM modes and propagation distances tested are correctly identified, only two images with $\ell = 3$, $z = 80$ cm are predicted to be $\ell = 3$, $z = 75$ cm in **Figure 4B**, and only two images with $\ell = 2$, $z = 40$ cm are predicted to be $\ell = 2$, $z = 45$ cm in **Figure 4C**.

Finally, we want to emphasize that using classical methods (e.g., interferometer) to analyze the distorted intensity images in **Figure 2B** is quite challenging. However, according to training and test results, our deep learning model can accurately identify vortex beams with varying topological charges and propagation distances even under the influence of severe turbulence. This demonstrates that our approach has a high level of robustness and is very useful for practical applications. We note that our approach can be adapted to identify larger ℓ value with longer and more accurate transmission distance. However, due to the limitation of our equipment, such as the resolution of SLM and CCD, as well as the experimental error caused by the laboratory environment, we limit the size of our topological charges and the length of the propagation distance. We believe our designed deep learning neural network does not fundamentally limit the recognition accuracy, and its potential is far from being reached. Moreover, our scheme can be adapted to many vortex beam related applications. For instance, we can adapt our work to consider multiple types of vortex beams, and even the combination of them. Furthermore, the accurate identification of the propagation distance might be a novel technique for sensing related applications. Last but not least, our approach can be applied to free-space OAM communication, especially the demodulation system, to increase the robustness of the communication. We expect that by combining the unique characteristics of vortex beams with the advantages of the deep learning algorithm, more breakthroughs in vortex beams research can be made in the future.

CONCLUSION

Vortex beams have enormous potential due to their versatility and virtually unlimited quantum information resources. However, these beams are highly susceptible to undesirable experimental conditions such as propagation distance and phase distortions. In our work, we exploit the deep learning algorithm to identify a vortex beam's topological charge and propagation distance. Specifically, we focus on vortex beam with topological charge ℓ from 1 to 5, and the propagation distance z ranges from 40 to 100 cm. Additionally, we consider the effect of turbulence-induced in the propagation of the beam. We experimentally demonstrated that our customized deep learning algorithm could accurately identify the propagation distance and topological charge. Our work has important implications for the realistic implementation of OAM-based optical communications and sensing protocols in a turbulent environment.

DATA AVAILABILITY STATEMENT

The raw data supporting the conclusion of this article will be made available by the authors, without undue reservation.

AUTHOR CONTRIBUTIONS

The idea was conceived by R-BJ, CY, and HL. The experiment was designed by HL, YG, CY, and R-BJ. The experiment was performed by HL with help of R-BJ, CY, YG, Z-XY, CD, and W-HC. The theoretical description and numerical simulation were developed by YG, CY, and R-BJ. The deep learning process was carried out by HL. The data was analyzed by HL, YG, CY, and R-BJ. The project was supervised by R-BJ and CY. All authors contributed to the preparation of the manuscript.

FUNDING

This work is supported by the National Natural Science Foundations of China (Grant Nos.12074299, 91836102, 11704290) and by the Guangdong Provincial Key Laboratory (Grant No. GKLQSE202102).

ACKNOWLEDGMENTS

We thank Prof. Zhi-Yuan Zhou for the helpful discussion.

REFERENCES

1. Franke-Arnold S, Allen L, Padgett M. Advances in Optical Angular Momentum. *Laser Photon Rev* (2008) 2:299–313. doi:10.1002/lpor.200810007
2. Rubinsztein-Dunlop H, Forbes A, Berry MV, Dennis MR, Andrews DL, Mansuripur M, et al. Roadmap on Structured Light. *J Opt* (2016) 19: 013001. doi:10.1088/2040-8978/19/1/013001
3. Fickler R, Lapkiewicz R, Plick WN, Krenn M, Schaeff C, Ramelow S, et al. Quantum Entanglement of High Angular Momenta. *Science* (2012) 338:640–3. doi:10.1126/science.1227193
4. Bai Y, Lv H, Fu X, Yang Y. Vortex Beam: Generation and Detection of Orbital Angular Momentum [Invited]. *Chin. Opt. Lett.* (2022) 20:012601. doi:10.3788/col202220.012601
5. Friese MEJ, Nieminen TA, Heckenberg NR, Rubinsztein-Dunlop H. Optical Alignment and Spinning of Laser-Trapped Microscopic Particles. *Nature* (1998) 394:348–50. doi:10.1038/28566
6. Padgett M, Bowman R. Tweezers with a Twist. *Nat Photon* (2011) 5:343–8. doi:10.1038/nphoton.2011.81
7. Grier DG. A Revolution in Optical Manipulation. *Nature* (2003) 424:810–6. doi:10.1038/nature01935
8. Curtis JE, Grier DG. Structure of Optical Vortices. *Phys Rev Lett* (2003) 90: 133901. doi:10.1103/physrevlett.90.133901
9. Lavery MPJ, Speirits FC, Barnett SM, Padgett MJ. Detection of a Spinning Object Using Light's Orbital Angular Momentum. *Science* (2013) 341:537–40. doi:10.1126/science.1239936
10. Mair A, Vaziri A, Weihs G, Zeilinger A. Entanglement of the Orbital Angular Momentum States of Photons. *Nature* (2001) 412:313–6. doi:10.1038/35085529
11. Molina-Terriza G, Torres JP, Torner L. Twisted Photons. *Nat Phys* (2007) 3: 305–10. doi:10.1038/nphys607
12. Magaña-Loaiza OS, Boyd RW. Quantum Imaging and Information. *Rep Prog Phys* (2019) 82:124401. doi:10.1088/1361-6633/ab5005
13. Ding D-S, Zhang W, Zhou Z-Y, Shi S, Xiang G-Y, Wang X-S, et al. Quantum Storage of Orbital Angular Momentum Entanglement in an Atomic Ensemble. *Phys Rev Lett* (2015) 114:050502. doi:10.1103/physrevlett.114.050502
14. Langford NK, Dalton RB, Harvey MD, O'Brien JL, Pryde GJ, Gilchrist A, et al. Measuring Entangled Qutrits and Their Use for Quantum Bit Commitment. *Phys Rev Lett* (2004) 93:053601. doi:10.1103/physrevlett.93.053601
15. Zhang P, Ren X-F, Zou X-B, Liu B-H, Huang Y-F, Guo G-C. Demonstration of One-Dimensional Quantum Random Walks Using Orbital Angular Momentum of Photons. *Phys Rev A* (2007) 75:052310. doi:10.1103/physreva.75.052310
16. Nagali E, Sciarrino F, De Martini F, Marrucci L, Piccirillo B, Karimi E, et al. Quantum Information Transfer from Spin to Orbital Angular Momentum of Photons. *Phys Rev Lett* (2009) 103:013601. doi:10.1103/physrevlett.103.013601
17. Zhang P, Jiang Y, Liu R-F, Gao H, Li H-R, Li F-L. Implementing the Deutsch's Algorithm with Spin-Orbital Angular Momentum of Photon without Interferometer. *Opt Commun* (2012) 285:838–41. doi:10.1016/j.optcom.2011.11.024
18. Bozinovic N, Yue Y, Ren Y, Tur M, Kristensen P, Huang H, et al. Terabit-scale Orbital Angular Momentum Mode Division Multiplexing in Fibers. *Science* (2013) 340:1545–8. doi:10.1126/science.1237861
19. Wang J, Yang J-Y, Fazal IM, Ahmed N, Yan Y, Huang H, et al. Terabit Free-Space Data Transmission Employing Orbital Angular Momentum Multiplexing. *Nat Photon* (2012) 6:488–96. doi:10.1038/nphoton.2012.138
20. Ouyang X, Xu Y, Xian M, Feng Z, Zhu L, Cao Y, et al. Synthetic Helical Dichroism for Six-Dimensional Optical Orbital Angular Momentum Multiplexing. *Nat Photon* (2021) 15:901–7. doi:10.1038/s41566-021-00880-1
21. Zhang M, Ren H, Ouyang X, Jiang M, Lu Y, Hu Y, et al. Nanointerferometric Discrimination of the Spin-Orbit Hall Effect. *ACS Photon* (2021) 8:1169–74. doi:10.1021/acsphotonics.1c00087
22. Wang L, Jiang X, Zou L, Zhao S. Two-dimensional Multiplexing Scheme Both with Ring Radius and Topological Charge of Perfect Optical Vortex Beam. *J Mod Opt* (2018) 66:87–92. doi:10.1080/09500340.2018.1512669
23. Molina-Terriza G, Torres JP, Torner L. Management of the Angular Momentum of Light: Preparation of Photons in Multidimensional Vector States of Angular Momentum. *Phys Rev Lett* (2001) 88:013601. doi:10.1103/physrevlett.88.013601
24. Rodenburg B, Lavery MPJ, Malik M, O'Sullivan MN, Mirhosseini M, Robertson DJ, et al. Influence of Atmospheric Turbulence on States of Light Carrying Orbital Angular Momentum. *Opt Lett* (2012) 37:3735. doi:10.1364/ol.37.003735
25. Rodenburg B, Mirhosseini M, Malik M, Magaña-Loaiza OS, Yanakas M, Maher L, et al. Simulating Thick Atmospheric Turbulence in the Lab with Application to Orbital Angular Momentum Communication. *New J Phys* (2014) 16:033020. doi:10.1088/1367-2630/16/3/033020
26. Paterson C. Atmospheric Turbulence and Orbital Angular Momentum of Single Photons for Optical Communication. *Phys Rev Lett* (2005) 94:153901. doi:10.1103/physrevlett.94.153901
27. Tyler GA, Boyd RW. Influence of Atmospheric Turbulence on the Propagation of Quantum States of Light Carrying Orbital Angular Momentum. *Opt Lett* (2009) 34:142. doi:10.1364/ol.34.000142
28. Ndagano B, Mphuthi N, Milione G, Forbes A. Comparing Mode-Crosstalk and Mode-dependent Loss of Laterally Displaced Orbital Angular Momentum and Hermite-Gaussian Modes for Free-Space Optical Communication. *Opt Lett* (2017) 42:4175. doi:10.1364/ol.42.004175
29. Krenn M, Fickler R, Fink M, Handsteiner J, Malik M, Scheidl T, et al. Communication with Spatially Modulated Light through Turbulent Air across vienna. *New J Phys* (2014) 16:113028. doi:10.1088/1367-2630/16/11/113028
30. Cox MA, Maqondo L, Kara R, Milione G, Cheng L, Forbes A. The Resilience of Hermite- and Laguerre-Gaussian Modes in Turbulence. *J Lightwave Technol* (2019) 37:3911–7. doi:10.1109/jlt.2019.2905630
31. Courtial J, Dholakia K, Robertson DA, Allen L, Padgett MJ. Measurement of the Rotational Frequency Shift Imparted to a Rotating Light Beam Possessing Orbital Angular Momentum. *Phys Rev Lett* (1998) 80:3217–9. doi:10.1103/physrevlett.80.3217
32. Zhang W, Qi Q, Zhou J, Chen L. Mimicking Faraday Rotation to Sort the Orbital Angular Momentum of Light. *Phys Rev Lett* (2014) 112:153601. doi:10.1103/physrevlett.112.153601
33. Padgett M, Arlt J, Simpson N, Allen L. An experiment to Observe the Intensity and Phase Structure of Laguerre-Gaussian Laser Modes. *Am J Phys* (1996) 64: 77–82. doi:10.1119/1.18283
34. Yongxin L, Hua T, Jixiong P, Baida L. Detecting the Topological Charge of Vortex Beams Using an Annular triangle Aperture. *Opt Laser Tech* (2011) 43: 1233–6. doi:10.1016/j.optlastec.2011.03.015
35. Karimi E, Piccirillo B, Nagali E, Marrucci L, Santamato E. Efficient Generation and Sorting of Orbital Angular Momentum Eigenmodes of Light by Thermally Tuned Q-Plates. *Appl Phys Lett* (2009) 94:231124. doi:10.1063/1.3154549
36. Shin H-C, Roth HR, Gao M, Lu L, Xu Z, Nogues I, et al. Deep Convolutional Neural Networks for Computer-Aided Detection: CNN Architectures, Dataset Characteristics and Transfer Learning. *IEEE Trans Med Imaging* (2016) 35: 1285–98. doi:10.1109/tmi.2016.2528162
37. Quattoni A, Collins M, Darrell T. Transfer Learning for Image Classification with Sparse Prototype Representations. In: IEEE Conference on Computer Vision and Pattern Recognition. IEEE (2008). doi:10.1109/cvpr.2008.4587637
38. Taigman Y, Yang M, Ranzato M, Wolf L. Deepface: Closing the gap to Human-Level Performance in Face Verification. In: Proceedings of the IEEE Conference on Computer Vision and Pattern Recognition. Columbus: CVPR (2014). doi:10.1109/cvpr.2014.220
39. Melnikov AA, Poulsen Nautrup H, Krenn M, Dunjko V, Tiersch M, Zeilinger A, et al. Active Learning Machine Learns to Create New Quantum Experiments. *Proc Natl Acad Sci USA* (2018) 115:1221–6. doi:10.1073/pnas.1714936115
40. Doster T, Watnik AT. Machine Learning Approach to OAM Beam Demultiplexing via Convolutional Neural Networks. *Appl Opt* (2017) 56: 3386. doi:10.1364/ao.56.003386
41. You C, Quiroz-Juárez MA, Lambert A, Bhusal N, Dong C, Perez-Leija A, et al. Identification of Light Sources Using Machine Learning. *Appl Phys Rev* (2020) 7:021404. doi:10.1063/1.5133846
42. Bhusal N, Lohani S, You C, Hong M, Fabre J, Zhao P, et al. Spatial Mode Correction of Single Photons Using Machine Learning. *Adv Quan Tech* (2021) 4:2000103. doi:10.1002/qute.202000103

43. Gibson G, Courtial J, Padgett MJ, Vasnetsov M, Pas'ko V, Barnett SM, et al. Free-space Information Transfer Using Light Beams Carrying Orbital Angular Momentum. *Opt Express* (2004) 12:5448. doi:10.1364/opex.12.005448
44. Liao K, Chen Y, Chen Y, Yu Z, Hu X, Wang X, et al. All-optical Computing Based on Convolutional Neural Networks. *Opto-Electron Adv* 4:200060 (2021). doi:10.29026/oea.2021.200060
45. Bhusal N, Hong M, Miller NR, Quiroz-Juarez MA, de J Leon-Montiel R, You C, et al. *Smart Quantum Statistical Imaging beyond the Abbe-Rayleigh Criterion*. arXiv:2110.05446 (2021).
46. Zhang C, Zhao Y. Orbital Angular Momentum Nondegenerate index Mapping for Long Distance Transmission. *IEEE Trans Wireless Commun* (2019) 18:5027–36. doi:10.1109/twc.2019.2927672
47. Krenn M, Handsteiner J, Fink M, Fickler R, Ursin R, Malik M, et al. Twisted Light Transmission over 143 Km. *Proc Natl Acad Sci USA* (2016) 113:13648–53. doi:10.1073/pnas.1612023113
48. Zhao SM, Leach J, Gong LY, Ding J, Zheng BY. Aberration Corrections for Free-Space Optical Communications in Atmosphere Turbulence Using Orbital Angular Momentum States. *Opt Express* (2011) 20:452. doi:10.1364/oe.20.000452
49. Zhou ZY, Zhu ZH, Liu SL, Liu SK, Wang K, Shi S, et al. Generation and Reverse Transformation of Twisted Light by Spatial Light Modulator. arXiv:1612.04482 (2016).
50. Collins SA. Lens-System Diffraction Integral Written in Terms of Matrix Optics. *J Opt Soc Am* (1970) 60:1168–77. doi:10.1364/JOSA.60.001168
51. Bos JP, Roggemann MC, Rao Gudimetla VS. Anisotropic Non-kolmogorov Turbulence Phase Screens with Variable Orientation. *Appl Opt* (2015) 54:2039–45. doi:10.1364/AO.54.002039
52. Glindemann A, Lane RG, Dainty JC. Simulation of Time-Evolving Speckle Patterns Using Kolmogorov Statistics. *J Mod Opt* (1993) 40:2381–8. doi:10.1080/09500349314552401
53. He K, Zhang X, Ren S, Sun J. Deep Residual Learning for Image Recognition. In: Proceedings of the IEEE Conference on Computer Vision and Pattern Recognition. Las Vegas: CVPR (2016). doi:10.1109/cvpr.2016.90
54. Kingma DP, Ba J. *Adam: A Method for Stochastic Optimization*. arXiv:1412.6980 (2014).
55. Fernando B, Habrard A, Sebban M, Tuytelaars T. *Subspace Alignment for Domain Adaptation*. arXiv:1409.5241 (2014).
56. Patel VM, Gopalan R, Li R, Chellappa R. Visual Domain Adaptation: A Survey of Recent Advances. *IEEE Signal Process Mag* (2015) 32:53–69. doi:10.1109/msp.2014.2347059
57. Krizhevsky A, Sutskever I, Hinton GE. ImageNet Classification with Deep Convolutional Neural Networks. *Commun ACM* (2017) 60:84–90. doi:10.1145/3065386
58. Liu Z, Yan S, Liu H, Chen X. Superhigh-resolution Recognition of Optical Vortex Modes Assisted by a Deep-Learning Method. *Phys Rev Lett* (2019) 123:183902. doi:10.1103/physrevlett.123.183902
59. Zhang Z, Sabuncu MR. Generalized Cross Entropy Loss for Training DeepNeural Networks with Noisy Labels. In: Proceedings of the 32nd International Conference on Neural Information Processing Systems. NY, USA: Red HookCurran Associates Inc. (2018). p. 8792–802.

Conflict of Interest: The authors declare that the research was conducted in the absence of any commercial or financial relationships that could be construed as a potential conflict of interest.